

Translocation of positively and negatively charged polystyrene nanoparticles in an in vitro placental model



Samantha K. Kloet ^{a,*}, Agata P. Walczak ^{a,b}, Jochem Louisse ^a, Hans H.J. van den Berg ^a, Hans Bouwmeester ^b, Peter Tromp ^c, Remco G. Fokkink ^d, Ivonne M.C.M. Rietjens ^a

^a Department of Toxicology, Wageningen University, Tuinlaan 5, 6703 HE Wageningen, The Netherlands

^b RIKILT – Wageningen UR, Wageningen, The Netherlands

^c TNO, Department of Applied Environmental Sciences, Princetonlaan 6, 3584 CB Utrecht, The Netherlands

^d Laboratory of Physical Chemistry and Colloid Science, Wageningen University, Wageningen, The Netherlands

ARTICLE INFO

Article history:

Received 19 January 2015

Revised 30 June 2015

Accepted 2 July 2015

Available online 3 July 2015

Keywords:

BeWo b30 cells

Placental translocation

Protein corona

Physico-chemical characteristics

ABSTRACT

To obtain insight in translocation of nanoparticles across the placental barrier, translocation was studied for one positively and two negatively charged polystyrene nanoparticles (PS-NPs) of similar size in an in vitro model. The model consisted of BeWo b30 cells, derived from a human choriocarcinoma grown on a transwell insert forming a cell layer that separates an apical from a basolateral compartment. PS-NPs were characterized with respect to size, surface charge, morphology and protein corona. Translocation of PS-NPs was not related to PS-NP charge. Two PS-NPs were translocated across the BeWo transwell model to a lower extent than amoxicillin, a model compound known to be translocated over the placental barrier to only a limited extent, whereas one PS-NP showed a slightly higher translocation. Studies on the effect of transporter inhibitors on the translocation of the PS-NPs indicated that their translocation was not mediated by known transporters and mainly dependent on passive diffusion. It is concluded that the BeWo b30 model can be used as an efficient method to get an initial qualitative impression about the capacity of NPs to translocate across the placental barrier and set priorities in further in vivo studies on translocation of NPs to the fetus.

© 2015 The Authors. Published by Elsevier Ltd. This is an open access article under the CC BY-NC-ND license (<http://creativecommons.org/licenses/by-nc-nd/4.0/>).

1. Introduction

Nanoparticles (NPs) are incorporated in a variety of consumer products, such as electronics, clothing, food, cosmetics and medicines. Consequently, there is an increasing potential for workers and consumers to be exposed to various NPs. Due to their small size and relatively large surface area compared to volume, NPs have physico-chemical characteristics different from the bulk material (Auffan et al., 2009). Although these novel characteristics drive the development of numerous applications in many fields of technology and medicine, they may also have unforeseen (adverse) health effects (Oberdorster, 2004; Stampfli et al., 2011). It is known that size and surface functionalization are major factors that influence kinetics, including rate of uptake, distribution, and excretion of NPs, and thereby their possible toxicity (Bhattacharjee et al., 2013a; Oberdorster et al., 2005; Park et al., 2011; Sager and Castranova, 2009). In order to bypass in vivo toxicity testing of every type of NP, efficient in vitro research methods with

prognostic potential would be of great value. Therefore, suitable in vitro methods are needed that can be used to predict the in vivo kinetics of NPs in order to predict in vivo internal exposure. At present, research on transplacental transfer of nanomaterials and their effects on the placenta and the developing fetus is still in its infancy (Buerki-Thurnherr et al., 2012; Juch et al., 2013; Saunders, 2009). However, the fetus may be exposed to NPs upon translocation across the placenta, (Menjoge et al., 2011). The aim of the present study was to obtain insight in translocation of NPs across the placental barrier by studying translocation of positively and negatively charged polystyrene NPs (PS-NPs) across an in vitro model. The model consisted of BeWo b30 cells, derived from a human choriocarcinoma, grown on a transwell insert forming a cell layer that separates an apical compartment from a basolateral compartment. When grown on transwell inserts, BeWo b30 cells retain functional adenosine triphosphate binding cassette (ABC) transporters specific to the apical and basolateral membranes, such as P-glycoprotein (Pgp), breast cancer resistance protein (BCRP) or multidrug resistance-associated protein 1 (MRP-1) (Atkinson et al., 2003; Ceckova et al., 2006; Evseenko et al., 2006; Milane et al., 2009; Mitra and Audus, 2010; Utoguchi et al., 2000;

* Corresponding author.

E-mail address: samantha.kloet@wur.nl (S.K. Kloet).

Wick et al., 2010). Furthermore, these cells express placental differentiation markers, such as human chorionic gonadotrophin (HCG) (Takeuchi et al., 1990) and the major cytochrome P450 isoforms (CYP1A1 and 1A2) present in placenta (Avery et al., 2003). In our previous studies the BeWo b30 transwell model was shown to be useful to study placental translocation of drugs and nutrients, and translocation of these compounds across the BeWo b30 layer in the transwell model appeared to correlate with their translocation in an ex vivo human placental model (Li et al., 2013). In the present study the BeWo b30 transwell model was used to study possible placental translocation of NPs. The model NPs selected for this study were 50 nm PS-NPs with positive or negative charge. PS-NPs are used in various products like food packaging, drug delivery systems, sensors, paints and electronics spacers in LCD displays (Arora and Padua, 2010; Chiu et al., 2015; Lee et al., 2014; Phosphorex; Simon et al., 2008). PS-NPs were characterized by measuring their size and polydispersity index (PDI) by dynamic light scattering (DLS), their surface potential (as an indication of surface charge) by ζ -potential measurements, their protein corona by SDS-PAGE and their morphology by scanning electron microscopy (SEM).

2. Materials and methods

2.1. Chemicals

Fluorescent red PS-NPs were obtained from Magsphere Inc. (Cat nr: AMFR050NM, CAFR050NM). Fluorescent Yellow-Green carboxylated 50 nm microspheres were obtained from Polysciences (Cat nr. 16661-10). 3-(4,5-Dimethylthiazol-2-yl)-2,5-diphenyltetrazolium bromide (MTT), fluorescein, antipyrine, amoxicillin, β -mercaptoethanol and Dulbecco's modified Eagle's medium (DMEM) (Cat nr. D5071 and D5671) were purchased from Sigma-Aldrich (Zwijndrecht, The Netherlands). Penicillin-streptomycin, L-glutamine, trypsin-EDTA, fetal calf serum (FCS), phosphate-buffered saline (PBS), and Hank's balanced salt solution (HBSS) were obtained from Invitrogen (Breda, The Netherlands). Laemmli Sample Buffer, Precision Plus Protein Dual Color Standards marker, Bio-Safe Coomassie Stain G-250 and Mini-PROTEAN TGX Gels were obtained from Bio-rad (Veenendaal, The Netherlands).

2.2. Cell culture

The choriocarcinoma BeWo cell line (clone b30) was kindly provided by the Institute of Public Health of the Faculty of Health Sciences (University of Copenhagen, Denmark) with permission from Dr. Alan Schwartz (Washington University, St. Louis, MO) and confirmed to be mycoplasma negative. Cells were cultured at 37 °C with 5% CO₂ in a humidified atmosphere in DMEM supplemented with 10% (v/v) heat inactivated FCS, 1% (v/v) penicillin-streptomycin and 1% (v/v) L-glutamine. Cells were subcultured every 3–4 days when reaching 80% confluence using trypsin-EDTA after rinsing with PBS.

2.3. Particle characterization

The size (hydrodynamic diameter) of the PS-NPs was determined by dynamic light scattering (DLS) using a Cobolt Samba 300 mW DPSS laser at a wavelength of 532 nm as a light source. Measurements were performed on freshly prepared NP solutions at 10 µg/ml in nanopure water and in cell culture medium containing 10% FCS. For each sample, twenty measurements were made and the detector intensity data (measured with an ALV/SO SIPD Single Photon Detector with ALV Static and Dynamic Fiber optics)

were processed with an ALV5000/60X0 external correlator and ALV-5000/E software (all from ALV-GmbH, Germany). Data were analyzed with the AfterALV software and mean diameter and polydispersity index (PDI) were determined for each PS-NP sample. Additionally the ζ -potential of the PS-NPs was measured at a concentration of 100 µg/ml using the Malvern Zetasizer 2000 (Malvern Instruments, UK). Three independent measurements, each containing 5 sub-measurements, were used to establish the average ζ -potential and standard deviation (SD) for each sample. Morphology of the PS-NPs was characterized by scanning electron microscopy (SEM). To this end suspensions of the PS-NPs (20 µg/ml) in water were studied using SEM. Of each suspension 20 µl was deposited on a nickel-coated polycarbonate filter, which was mounted on an aluminum specimen holder. The droplets were left to dry. Subsequently the filters with PS-NPs were coated with a 5 nm layer of chromium with an Emitech K575X turbo sputter coater. The high resolution field emission gun scanning electron microscope (FESEM) used in this study was a Tescan MIRA-LMH FESEM (Tescan, Brno, Czech Republic). The microscope was operated at an accelerating voltage of 15 kV, working distance (WD) of 10 mm and spot size of 5 nm. The mean diameter \pm SD of 50–500 particles is given.

2.4. Protein corona detection

For the protein corona characterization, methods were adapted from previous similar studies (Lesniak et al., 2010; Lundqvist et al., 2008). Briefly, PS-NPs were suspended in DMEM cell culture medium containing 10% FCS at a concentration of 1.66 mg/ml and incubated for 24 h at 37 °C. The samples were centrifuged 40 min at 18,000 rcf at 15 °C to pellet the NP-protein complexes. The pellet was resuspended in 1 ml PBS, transferred to a new tube and centrifuged again. This washing procedure was repeated three times to eliminate non-firmly bound proteins, using a new tube in every wash step to avoid artifacts from proteins bound to the tube wall. Finally, after the last centrifugation, the supernatant was removed and the pellets were resuspended carefully with 70 µl of a 1:1 (v/v) mixture of PBS and 2× Laemmli Sample Buffer containing 5% β -mercaptoethanol. Next, the samples were boiled for 5 min at 98 °C to denature the proteins and unbind the proteins from the PS-NPs and then cooled down immediately on ice. Samples were again centrifuged 40 min at 18,000 rcf at 15 °C to separate the PS-NPs from proteins desorbed from their surface. Of the supernatant containing the desorbed proteins 20 µl was loaded on the gel. In this way the amount of protein loaded in each lane was normalized for the weight of the different PS-NPs in the sample. A second gel was loaded with samples that were normalized for amount of protein in each lane. As we could not measure the protein content because of interference of β -mercaptoethanol which was present and required in all samples, an indirect measurement of total protein present in the samples was used. To this end the acquired gel image of the first gel was digitally analyzed for the pixel intensity of each whole lane. We thus obtained an estimate of the amount of protein loaded in each sample. The pixel intensity of all lanes was expressed relative to the pixel intensity of the lane with the lowest pixel intensity. This resulted in a factor by which the samples should be diluted in order to load the same amount of protein in all lanes of the second gel. One-dimensional polyacrylamide gel electrophoresis was performed using standard methods on the Bio-Rad Mini-Protean system, at 90 V for about 80 min, until the proteins neared the end of the gel (Mini-PROTEAN TGX Gel, 12% polyacrylamide 1 mm). A marker sample was included on each gel. The gels were washed in 40% methanol in water containing 10% acetic acid for 15 min and subsequently stained with Bio-Safe Coomassie Stain G-250 for 1.5 h. Afterward, the gels were washed extensively and stored overnight in distilled water. Gels

were scanned using the Odyssey scanner (Li-cor ISO 9001) and analyzed by further quantification of the band intensity of the lanes with the Odyssey software (Li-cor Biosciences). Experiments were repeated three times.

2.5. MTT assay

BeWo b30 cells were seeded at 1×10^4 cells/well in 100 μl culture medium in 96-well plates and incubated at 37 °C and 5% CO₂ for 24 h, followed by exposure to 100 μl of PS-NP solutions with concentrations ranging from 0 $\mu\text{g}/\text{ml}$ to 100 $\mu\text{g}/\text{ml}$. After 24 h 10 μl of MTT solution in PBS (5 mg/ml) was added to the medium to reach a final concentration of 0.5 mg/ml MTT. After 1.5 h incubation, the MTT solution was removed and 100 μl /well pure DMSO were added to lyse the cells and to dissolve the formazan crystals. The plates were shaken for 10 min protected from light and subsequently absorbance was measured at 562 and 620 (background) nm using a SpectraMax M2 Microplate Reader (Molecular Devices LLC, Sunnyvale, CA USA). For each PS-NP concentration cellular MTT reduction to formazan is expressed as percentage of the corresponding DMEM control reading (0 $\mu\text{g}/\text{ml}$). The absence of possible interference of particle fluorescence with the absorbance readings was confirmed by reading the absorbance of wells with different concentrations of NPs after adding MTT and this indicated there was no interference of the particles with the absorbance readings.

2.6. Translocation studies

Originally transwell membranes are coated with placental collagen before seeding the BeWo b30 cells (Bode et al., 2006). However, previous studies showed that this collagen coating inhibits NP transfer across the permeable membrane (Cartwright et al., 2012). Therefore, no collagen coating was used in the translocation studies. This will present a model presenting the highest possible translocation and thus preventing underestimation of the translocation. BeWo b30 cells were seeded at a density of 100,000 cells/cm² on 12-well transwell inserts containing a polycarbonate membrane (0.4 μm pore size and a surface area of 1.12 cm²) (Corning, NY, product number 3401) with daily refreshment of the medium as described by (Poulsen et al., 2009). At day 6 post-seeding the BeWo b30 cell layers were washed twice with prewarmed (37 °C) HBSS without phenol red after which transepithelial electrical resistance (TEER) measurements were performed just before exposure using a Millicell ERS-2 Volt-Ohm Meter (Millipore, USA). Cell layers showing TEER values >160 ohm cm² were chosen for translocation experiments, as these were values reported by others indicating a intact barrier (Li et al., 2013; Liu et al., 1997). After TEER measurement, HBSS was removed and replaced by exposure medium.

Translocation of the two reference compounds amoxicillin and antipyrine (both at final concentration 100 μM) was assessed by adding apically 0.5 ml of the test compound dissolved in HBSS and basolaterally 1.5 ml of HBSS. In order to ensure the quality of the BeWo model, we always include both antipyrine and amoxicillin in our transport studies, using the circumstances (HBSS without protein) as used in our validation study (Li et al., 2013). In that study, (Li et al., 2013) showed that the transport of antipyrine and amoxicillin is not affected by the presence of proteins in the medium. At selected time points a sample of 0.2 ml was taken from the basolateral compartment and replaced by an equal volume of HBSS. At the end of each experiment 0.2 ml was also taken from the apical compartment. Subsequently cells were washed three times with HBSS without phenol red, TEER values were determined to check for an intact barrier. If the TEER value after the translocation study was not lower than before the translocation study, the

experiment was considered valid, and the membrane with cells was dissected and transferred to an Eppendorf tube containing 250 μl 65% (v/v) methanol to determine the amount of compound accumulated in the cells using HPLC.

Translocation of PS-NPs in time was tested by adding 0.5 ml of the freshly prepared vortexed PS-NP dilutions in phenol red free DMEM supplemented with 10% FCS to the apical compartment. At selected time points, samples of 100 μl were taken from the apical and basolateral compartments and at the end of the incubation the membranes with BeWo b30 cell layers were washed three times with HBSS (37 °C) without phenol red and TEER values were measured to check cell layer integrity. Then membranes were dissected and transferred to an Eppendorf tube containing 400 μl cold nanopure water. Samples were sonicated in order to lyse the cells and samples of 100 μl were taken and added to a 96 wells plate to measure fluorescence for PS-NP quantification. PS-NP quantification was done by fluorescence measurements using a calibration curve (Magsphere PS-NPs: $\lambda_{\text{ex}} = 540$, $\lambda_{\text{em}} = 630$, Polysciences PS-NPs $\lambda_{\text{ex}} = 485$, $\lambda_{\text{em}} = 530$) using a SpectraMax M2 Microplate Reader (Molecular Devices LLC, Sunnyvale, CA USA).

The role of specific transporters in the translocation of PS-NPs was tested by performing the translocation experiments in the presence or absence of the transporter inhibitors verapamil (inhibitor of PgP), KO143 (inhibitor of human breast cancer resistance protein; BCRP), MK571 (inhibitor of multidrug resistance-associated protein 1; MRP-1), chlorpromazine (inhibitor of caveolin-mediated endocytosis) or methyl-β-cyclodextrin (MβCD) (inhibitor of clathrin-mediated endocytosis). Table S1 presents an overview of the different transporter inhibitors used, their transporter specificity, their concentrations generally used in literature to study transporter inhibition and relevant references Bhattacharjee et al. (2013b), Brand et al. (2008), dos Santos et al. (2011), Ushigome et al. (2000), Ceckova et al. (2006). All inhibitors were diluted from a 250 times concentrated stock solution in DMSO in cell culture medium, except for MβCD which was diluted from a 250 times concentrated stock solution in PBS. Transporter inhibitors were also added to the basolateral compartment containing 1.5 ml culture medium, using the same concentrations as applied in the apical compartment. Subsequently, the plate was incubated in a humidified atmosphere with 5% CO₂ at 37 °C. After 24 h, samples of 100 μl were taken and PS-NPs were quantified by fluorescence measurements in the same way as previously described.

2.7. High performance liquid chromatography analysis

To determine the transport rate of amoxicillin and antipyrine, the collected samples were quantified using High Performance Liquid Chromatography (HPLC) as was described by (Li et al., 2013).

2.8. Data analysis

The apparent permeability coefficients (Papp; cm/s) were calculated according to:

$$\text{Papp} = (dQ/dt)/(A \times C_0)$$

In which dQ/dt is the transport velocity (nmol/s or $\mu\text{g}/\text{s}$) in the initial phase when appearance in the basolateral chamber is linear in time, A – the surface area of the membrane insert (cm²) and C_0 the initial concentration of the compound in the donor chamber (nmol/ml or $\mu\text{g}/\text{ml}$) (Artursson and Karlsson, 1991).

2.9. Statistical analysis

Each experiment was repeated at least three or four times and the results are shown as mean \pm standard deviation (SD). Statistical analyses were performed using GraphPad Prism®

version 5, using a one-way analysis of variance ANOVA test and *post hoc* Tukey test to determine significant differences between the groups. Groups were considered significantly different when $p < 0.05$.

3. Results

3.1. Physico-chemical characterization of the PS-NPs

This study included three types of PS-NPs, one 50 nm positively charged PS-NP and two 50 nm negatively charged PS-NPs. The two 50 nm negatively charged PS-NPs were included because previous studies of our group revealed that these are translocated to a different extent across a Caco-2 monolayer (Walczak et al., 2014). Several physico-chemical properties of the nanoparticles were characterized.

SEM pictures of the PS-NPs (Fig. 1) confirm the spherical shape of the particles and their diameter of around 50 nm, although smaller particles can be observed in all samples. Automatic diameter measurements of these desiccated PS-NPs show that their sizes range between 15 and 75 nm with a mean value at 31.6 nm, 35 nm and 50.6 nm for the negatively charged

(Polysciences), negatively charged (Magsphere) and positively charged (Magsphere) PS-NPs respectively (Table S2).

The hydrodynamic diameters of the hydrated NPs were measured by dynamic light scattering (DLS) in nanopure water and in the culture medium containing 10% FCS as used for the translocation experiments (Table 1). The measured sizes of the PS-NPs in nanopure water were close to the sizes reported by the manufacturer. Upon addition of the positively charged PS-NPs to DMEM with 10% FCS, their size increased 1.5-fold. The measured sizes of the negatively charged PS-NPs (Magsphere) and negatively charged PS-NPs (Polysciences) in DMEM with 10% FCS increased slightly by 1.4 and 1.1 fold, respectively (Table 1). It is of interest to note that DLS analysis of medium with 10% FCS alone revealed that proteins from the FCS appear to form particles of comparable sizes as the NPs (Fig. S1). Formation of protein complexes in the nm range have been reported before (Liu et al., 2013a). Thus, DLS measurements of NPs in medium containing 10% FCS may be hampered by the protein aggregates of comparable size.

The surface charges of the positively and negatively charged PS-NPs were measured in nanopure water and in DMEM with 10% FCS by determining the zeta potential (Table 2). Positively charged PS-NPs had a zeta potential of +51.0 mV in nanopure water. Negatively charged PS-NPs of Magsphere and Polysciences

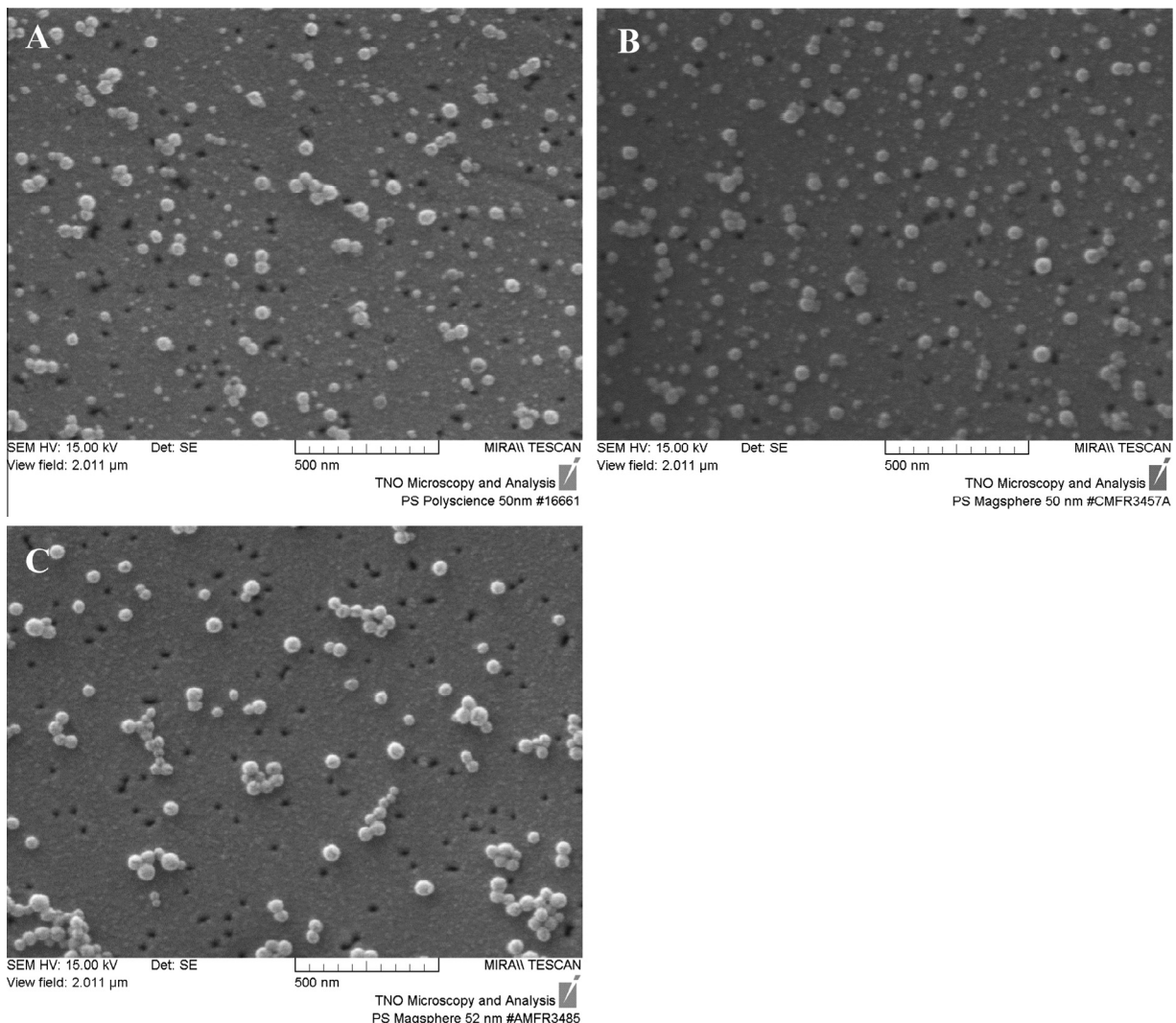


Fig. 1. SEM pictures of (A) 50 nm negatively charged PS-NP (Polysciences), (B) 50 nm negatively charged PS-NP (Magsphere) and (C) 50 nm positively charged PS-NP (Magsphere).

Table 1

DLS data of 50 nm PS-NPs with positive or negative charge in nanopure water and in medium with 10% FCS.

Nanoparticle	Medium	Mean size in nm (SD)	Polydispersity index (PDI)
50 nm positively charged PS-NP (Magsphere)	Nanopure water	56.5 (3.02)	0.09
	DMEM + FCS	82.7 (30.91)	0.49
50 nm negatively charged PS-NP (Magsphere)	Nanopure water	50.4 (1.74)	0.19
	DMEM + FCS	69.0 (10.1)	0.49
50 nm negatively charged PS-NP (Polysciences)	Nanopure water	52.4 (0.1)	0.21
	DMEM + FCS	57.6 (11.7)	0.50

Table 2

Zeta potential of 50 nm PS-NPs with positive or negative charge in nanopure water and in medium with 10% FCS, and zeta potential measured with medium with 10% FCS.

Nanoparticle	Medium	Mean zeta (mV)	SD
50 nm positively charged PS-NP (Magsphere)	Nanopure water	51	4.5
	DMEM + FCS	-12.0	1.2
50 nm negatively charged PS-NP (Magsphere)	Nanopure water	-55.5	6.7
	DMEM + FCS	-11.1	0.9
50 nm negatively charged PS-NP (Polysciences)	Nanopure water	-58.3	2.7
	DMEM + FCS	-10.9	0.2
None	DMEM + FCS	-9.16	1.3

have a zeta potential of -55.5 mV and -58.3 mV respectively in nanopure water. In medium with 10% FCS all NPs get a similar slightly negative charge. This may be explained by the fact that the majority of particles present in these samples are protein aggregates from the 10% FCS so that the zeta potential may reflect the overall charge of the protein aggregates rather than those of the PS-NPs (Table 2). Alternatively the similar charges in the presence of FCS may be ascribed to the protein corona dominating the overall charge.

3.2. Protein corona detection

Fig. 2A shows a representative picture of the SDS-PAGE gel with proteins desorbed from the different PS-NPs after their incubation in medium with 10% FCS. Each lane contains the amount of protein obtained from the same amount of PS-NP and thus, given the similar size of the PS-NPs, presents the amount of protein desorbed from a presumably similar surface area of the PS-NPs. Proteins desorbed from the protein corona of NPs are present in lanes 2–4. Fig. 2B shows a protein gel prepared to contain the same amount of protein in each lane. The band intensities of the lanes containing NPs were further quantified using the Odyssey software and graphs thus obtained are also presented in Fig. 2. These results reveal differences in the amount but not the nature of the proteins in the corona of the three different PS-NPs (Fig. 2A + B lanes 2–4). From the 50 nm positively charged PS-NPs (lane 3) only a small amount of protein corona was obtained. The control (lane 5) shows the DMEM sample without nanoparticles which was treated by the same experimental procedure as NP samples. Hardly any protein is detected in this control, which corroborates that the proteins which are detected in the other samples are coming from the protein corona of the PS-NPs. Lane 6 shows the proteins present in the medium containing 10% FCS and comparison of this pattern to that of the PS-NPs reveals that not all medium proteins contribute to the protein corona to the same relative extent at which they are present in the medium, indicating at least some preferential binding of proteins to the NPs.

3.3. Cell viability studies

Before testing the transplacental translocation of the PS-NPs, the concentration of the PS-NPs to be tested in the BeWo b30

transwell translocation studies were chosen based on results from cell viability studies. The cell viability of BeWo b30 cells upon 24 h exposure to increasing PS-NP concentrations was determined using the MTT assay. Only cells exposed to the positively charged PS-NPs showed a decrease in MTT reduction, an effect that becomes statistically significant at concentrations of $20\text{ }\mu\text{g/ml}$ and higher (Fig. 3), whereas no effect was found upon exposure to the negatively charged PS-NPs. Based on these results the concentration of PS-NPs to be tested in the translocation studies was chosen at $10\text{ }\mu\text{g/ml}$.

3.4. Placental translocation of model compounds

In order to calibrate the BeWo b30 model system and provide points for comparison the translocation of two model compounds antipyrine and amoxicillin was determined. These compounds are known to be translocated across the placenta and also across the BeWo cell layer in vitro at respectively high or low rate (Akbaraly et al., 1985; Li et al., 2013). Table 3 shows the apparent permeability coefficients for antipyrine and amoxicillin amounting to $53 \times 10^{-6}\text{ cm/s}$ for antipyrine and $5.1 \times 10^{-6}\text{ cm/s}$ for amoxicillin indicating that the translocation of these two model compounds varies by one order of magnitude. Previously it was reported that for a series of model compounds including antipyrine and amoxicillin a good correlation ($r^2 = 0.95$) exists between their relative transport in the BeWo b30 transwell model and their transport in an ex vivo placental perfusion model (Li et al., 2013) and that also in the ex vivo placental transport model antipyrine and amoxicillin showed a difference in transport rate of about one order of magnitude (Akbaraly et al., 1985).

3.5. Placental translocation of PS-NPs

The time-dependent translocation of the three PS-NPs to the basolateral compartment was determined using an apical concentration of $10\text{ }\mu\text{g/ml}$ PS-NP (Fig. 4). Upon 24 h incubation the negatively charged PS-NPs from Magsphere were not detected in the basolateral compartment. For the other two PS-NPs a time dependent increase in the basolateral compartment was observed (Fig. 4). The apparent permeability coefficient of the positively charged PS-NPs from Magsphere was the lowest (Papp value of

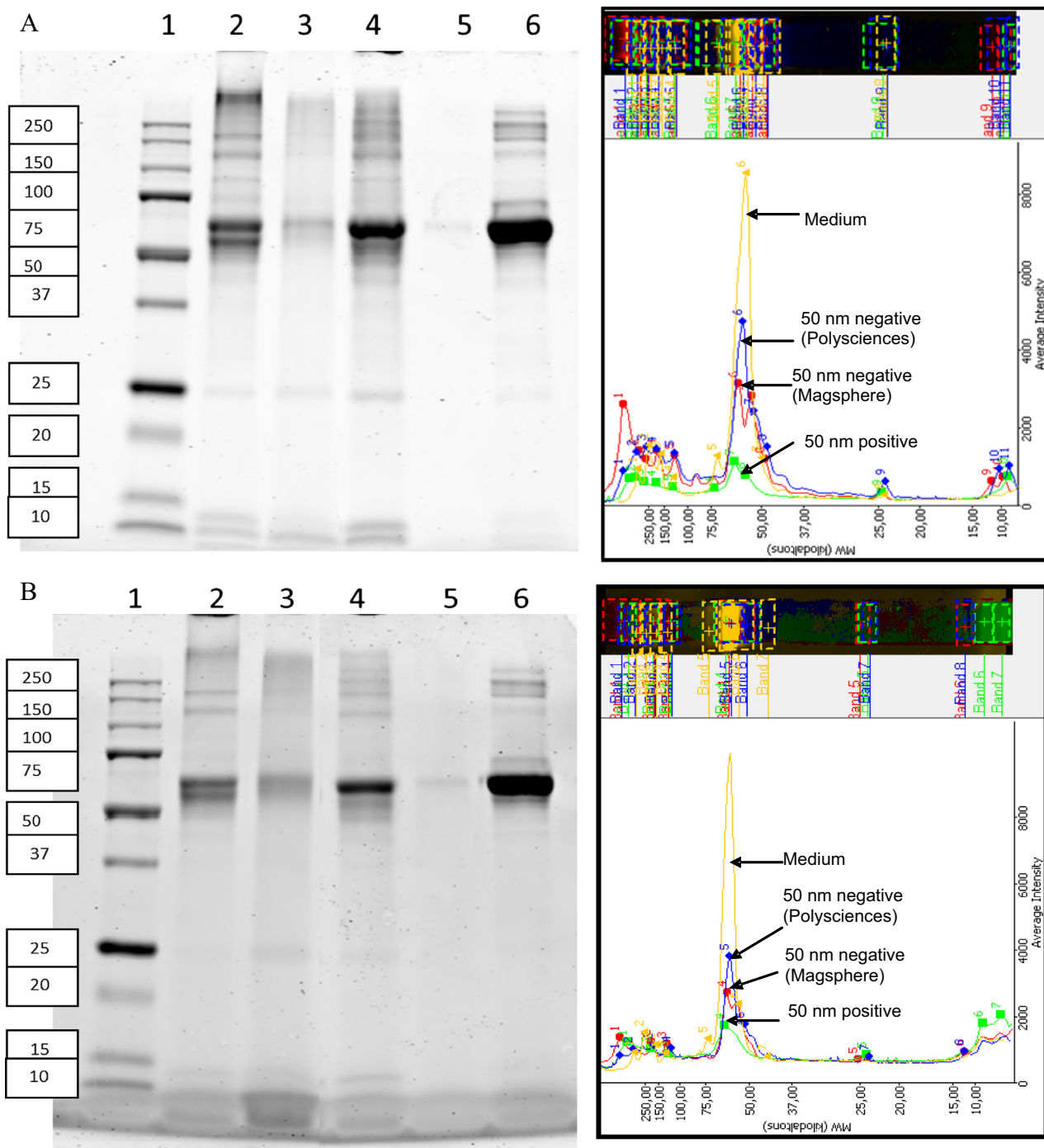


Fig. 2. SDS-PAGE gel showing the desorbed protein corona of different PS-NPs with the lanes containing: in gel (A) the amount of protein corresponding to the same surface area of the PS-NPs and those in gel (B) a similar amount of total protein. Lanes: (1) marker; (2) 50 nm negatively charged (Magsphere); (3) 50 nm positively charged (Magsphere); (4) 50 nm negatively charged (Polysciences); (5) Control: medium sample without NPs which followed the same experimental procedure as the NP-samples; (6) Medium. The right part of the figure shows the banding pattern of lanes 2–4 and 6.

0.3×10^{-6} cm/s), followed by that of the negatively charged PS-NPs from Polysciences (Papp value of 13×10^{-6} cm/s). In the absence of cells, PS-NP translocation across the insert was much higher which corroborates that the BeWo b30 cell layer acts as a barrier.

Comparison of the apparent permeability coefficients of the PS-NPs that were translocated with that of the reference compound amoxicillin, known to be translocated over the placental barrier to only a limited extent, reveals that translocation of the positively charged PS-NPs of Magsphere is 17 fold lower than that

of amoxicillin, whereas the translocation of the negatively charged PS-NPs from Polysciences was 2.5 fold higher than that of amoxicillin (Table 3).

3.6. Compartmental distribution of PS-NPs in the presence of transporter inhibitors

To investigate the possible role of specific transport mechanisms in the translocation of the PS-NPs across BeWo b30 cell layers, the distribution of the NPs over the three compartments

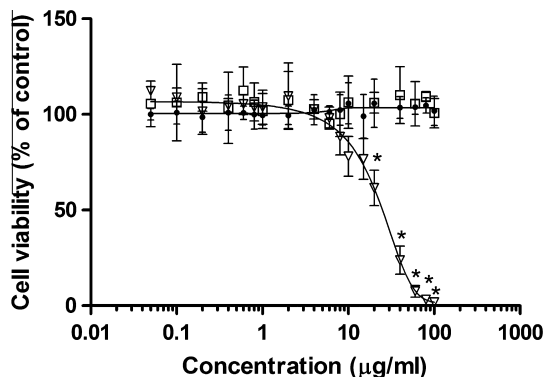


Fig. 3. Effects of three different PS-NPs on cell viability of BeWo b30 cells as determined with the MTT assay. BeWo b30 cells were exposed for 24 h to increasing concentrations of 50 nm positively charged PS-NP (Magsphere) (open triangle) or 50 nm negatively charged PS-NP (Magsphere) (closed circle) or 50 nm negatively charged PS-NP (Polysciences) (open square) PS-NPs. Data are expressed as percentage of the negative control and presented as the mean \pm SD of $n = 3$ independent biological replicates. The * indicates $p < 0.05$ for a significant difference with the other two types of PS-NPs ($n = 3$).

Table 3

Apparent permeability (Papp) coefficients across BeWo b30 cell barrier of the reference compounds antipyrine and amoxicillin, and the PS-NPs. Data presented are the mean \pm SD of $n = 3$ independent biological replicates.

	Mean Papp value \pm SD (cm/s)
Antipyrine	$53 \times 10^{-6} \pm 5.6 \times 10^{-6}$
Amoxicillin	$5.1 \times 10^{-6} \pm 0.52 \times 10^{-6}$
50 nm positively charged PS-NP (Magsphere)	$0.3 \times 10^{-6} \pm 0.05 \times 10^{-6}$
50 nm negatively charged PS-NP (Magsphere)	ND
50 nm negatively charged PS-NP (Polysciences)	$13 \times 10^{-6} \pm 1.1 \times 10^{-6}$

* ND: not detected, so no Papp coefficient derived.

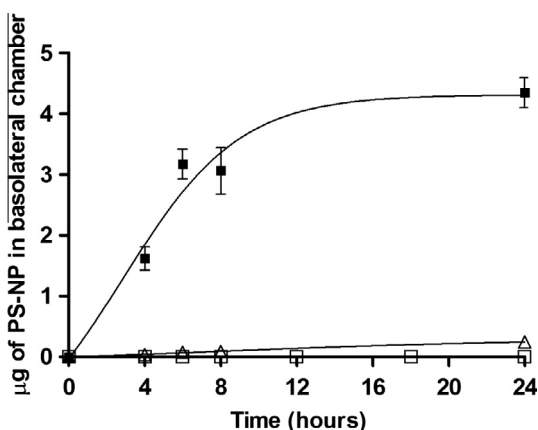


Fig. 4. Time dependent translocation across the BeWo b30 cell layer of 50 nm positively charged PS-NPs of Magsphere (open triangle), 50 nm negatively charged PS-NPs of Magsphere (open square) and 50 nm negatively charged PS-NPs of Polysciences (closed square) with starting concentration of 10 μ g/ml. Papp values (Table 3) were calculated from the linear part of the curve. Results presented are the mean \pm SD of $n = 3$ independent biological replicates.

(apical, basolateral and intracellular) was assessed in the presence or absence of inhibitors of endocytosis or of specific ABC transporters. Results obtained are presented in Fig. 5. For the positively charged PS-NPs, the presence of MK571, an inhibitor of MRP-1, slightly but significantly ($p < 0.01$) decreased the amount of PS-NPs in the apical compartment from 71.5% to 67.8% and

significantly increased ($p < 0.01$) the amount of PS-NPs in the basolateral compartment from 7.5% to 11.5% (Fig. 5A), indicating a 1.5 fold increased translocation across the BeWo b30 cell layer. TEER measurements performed after the distribution studies showed that the barrier integrity of the BeWo b30 cell layer was not affected, indicating that the increased translocation did not result from a compromised cell layer. Co-exposure to the positively charged PS-NPs and the BCRP- or PgP-inhibitors KO143 and verapamil, respectively, did not show an effect on the distribution of these PS-NPs (Fig. 5A). For the negatively charged 50 nm PS-NPs from Polysciences, none of the inhibitors showed a significant effect on the distribution of these particles in the BeWo transwell model (Fig. 5B) and the lack of intracellular signal indicates no intracellular localization. In addition, the clathrin and caveolin inhibitors (5 μ M chlorpromazine or 1 μ M M β CD, respectively) used to inhibit clathrin- and caveolin-mediated endocytosis, did not show an effect on translocation or distribution of any of the PS-NPs.

4. Discussion

To obtain insight in passage of NPs across the placental barrier, translocation of one positively and two different types of negatively charged PS-NPs across an in vitro model of the placental barrier was studied. The two negatively charged PS-NPs were included because previous studies within our group revealed they were translocated to a different extent across a Caco-2 monolayer, a model for intestinal translocation (Walczak et al., 2014). The model in the present study consisted of cells of the BeWo cell line (clone b30) grown on a transwell insert, and forming a cell layer that separates an apical compartment from a fetal compartment.

The characterization of the PS-NPs was done by measuring the size and polydispersity index (PDI) by dynamic light scattering (DLS), the ζ -potential (as an indication of surface charge) by ζ -potential measurements, the protein corona by SDS-PAGE and shape and the number-based size distribution by scanning electron microscopy (SEM). The results obtained reveal that in the presence of 10% FCS in cell culture medium, measurement of ζ -potential may be hampered by the presence of free protein particles as the ζ -potential of medium without or with PS-NPs present, resulted in the same negative ζ -potential. Alternatively the similar charges of the differently charged NPs in the presence of FCS may be ascribed to their protein corona dominating the underlying PS-NP's charge. SDS-PAGE analysis of this protein corona revealed that there were differences in mainly the amount but not in the nature of the proteins in the corona of the differently charged PS-NPs. The proteins desorbed from the PS-NPs were to a large extent a reflection of what was detected in the medium containing 10% FCS. This result was somewhat different from a previous study that reported that surface properties of PS-NPs significantly affected the composition of the protein corona (Lundqvist et al., 2008). In this latter study using different commercially available PS-NPs and mass spectrometry instead of SDS-PAGE, a fraction (about 35%) of the proteins in the corona were specifically detected on the positively charged PS-NPs or on the negatively charged PS-NPs, the others being similar.

In the present study it appeared that in spite of similar size (SEM and DLS), ζ -potential and type of proteins in the protein corona, the differently charged NPs displayed a remarkable difference in cytotoxicity, with only the PS-NPs with an original positive charge inducing cytotoxicity. The relatively higher cytotoxicity of positively as compared to negatively charged NPs was reported before for tri-block copolymer NPs (Bhattacharjee et al., 2012) but also for other type of NPs like gold NPs (Liu et al., 2013b) and silicon NPs (Bhattacharjee et al., 2013a). Thus for interaction

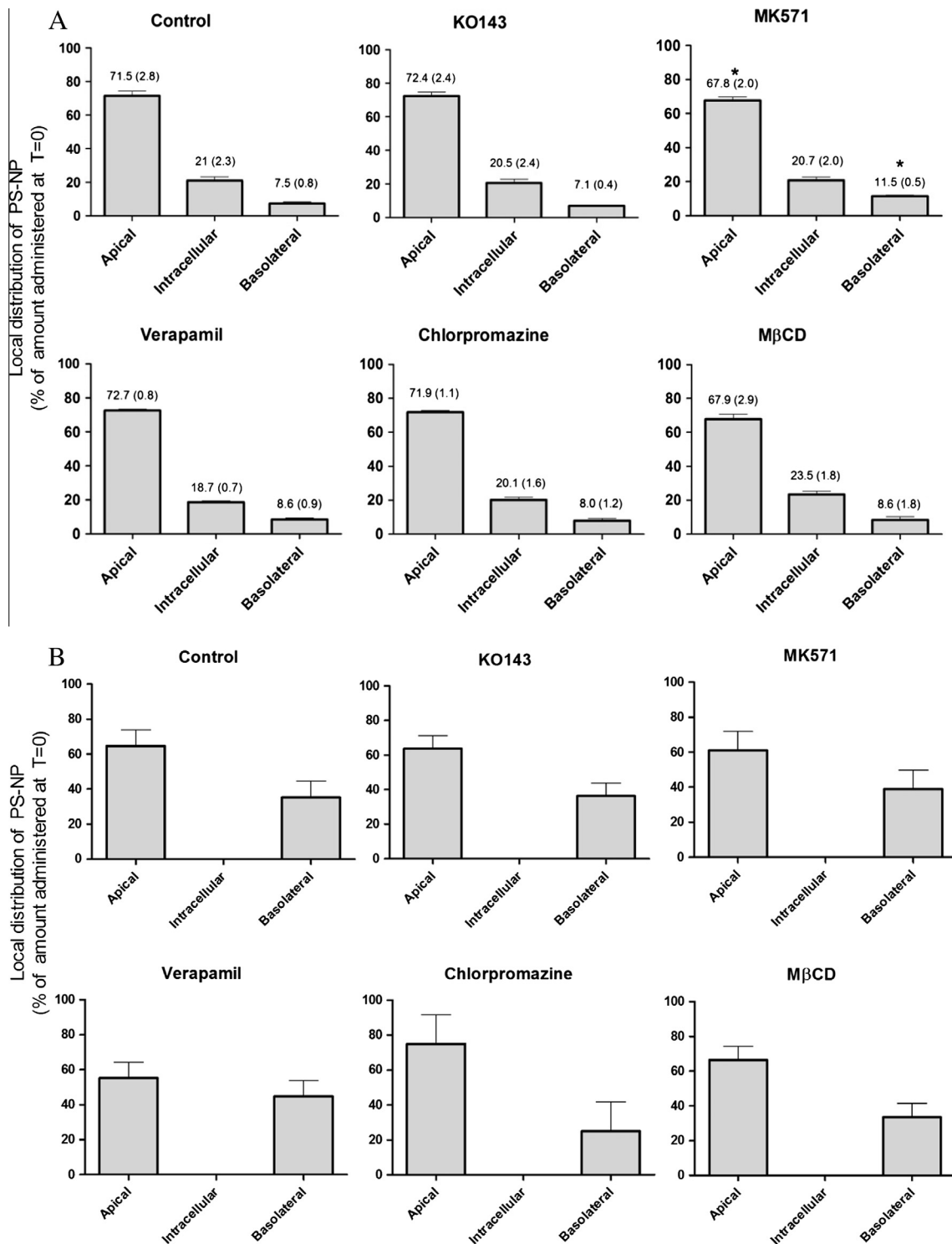


Fig. 5. Effect of specific transporter inhibitors (Table S1) on the distribution of (A) 50 nm positively charged PS-NPs of Magsphere; (B) 50 nm negatively charged PS-NP of Polysciences in the BeWo transwell model, 24 h after adding 0.5 ml of a 10 µg/ml PS-NP solution to the apical compartment. Results presented are the mean ± SD of $n = 4$ independent biological replicates. The * indicates a difference ($p < 0.01$) compared to the situation without inhibitors.

with the cells, the original difference in charges or surface chemistry of the particles as prepared and measured in water, is apparently still of influence. The higher cytotoxicity of positive NPs might be due to a stronger interaction with cells compared with negative NPs, because of the electrostatic attraction toward the negatively charged cell membrane (Kim et al., 2009).

Translocation of the different PS-NPs across the BeWo cell layer was not found to be related to PS-NP charge. A remarkable

difference in translocation was found between the two 50 nm negatively charged PS-NPs from different manufacturers. For the PS-NPs from Polysciences, the apparent permeability coefficient was slightly higher than that of amoxicillin, with a Papp value of 13×10^{-6} cm/s (Table 3). When testing the negatively charged PS-NPs from Magsphere, no PS-NPs could be detected in the basolateral compartment upon adding a concentration of 10 µg/ml in the apical compartment and 24 h incubation. A 30-fold difference

was found in translocation of the same types of negatively charged PS-NPs across a Caco-2 monolayer in a similar transwell model system (Walczak et al., 2014). Since none of the characterized parameters, including size, ζ -potential and protein corona revealed remarkable differences between the two negatively charged NPs, the difference may originate from the chemical groups on the surface of the NPs generating the negative charge. Although both PS-NPs are reported by the respective manufacturers to contain carboxylic groups from vinylic co-monomers, including acrylic acid, methacrylic acid and itaconic acid, further details on the chemical characteristics of the NP surface remained unknown. In this respect it is of interest that variation in steric shielding of the charge on a surface moiety due to subtle differences in the chemical structure of the charge bearing moiety may affect the cellular uptake and toxicity of fluorescent tri-block copolymer nanoparticles (Bhattacharjee et al., 2011). In this previous study it was demonstrated that three different positively charged tri-block copolymer nanoparticles showed different cellular uptake and toxicity in spite of a similar overall size and ζ -potential, and that only a different shielding of the charge due to subtle differences in the charge generating surface moiety influenced the cellular uptake and toxicity (Bhattacharjee et al., 2011). This factor may explain the different translocation rates of the two negatively charged 50 nm PS-NPs in this study, given the different carboxylic groups that have been used in the production of these different PS-NPs.

The translocation studies presented in this study revealed that the PS-NPs were translocated across the BeWo b30 transwell model to only a limited extent. We compared these results to reports in the literature studying the translocation of NPs across the placental barrier. A few studies also applied the BeWo b30 transwell model studying translocation of PEGylated gold NPs of 10–30 nm (Myllinen et al., 2008), iron oxide and silica NPs of 23–38 nm (Correia Carreira et al., 2013), dexamethasone loaded PLGA NPs of 140–289 nm (Ali et al., 2013), rhodamine labeled silica NPs of 25 and 50 nm (Sonsgaard Poulsen et al., 2013) and polystyrene NPs of 50 and 100 nm (Cartwright et al., 2012). These studies generally report that the NPs are translocated across the BeWo cell layer after a few hours of incubation to the basolateral compartment albeit in relatively small amounts. The results of the present study are in line with these observations, and suggest that translocation of NPs across the in vitro placental barrier cannot be excluded. Literature data obtained in ex vivo human placental perfusion models also report the potential of NPs to cross the placental barrier (Grafmuller et al., 2013; Menjoge et al., 2011; Sonsgaard Poulsen et al., 2013; Wick et al., 2010) and are in line with this conclusion.

In order to investigate the role of specific transporters in the translocation of the PS-NPs across the BeWo b30 cell layer, translocation studies were also performed in the absence and presence of transporter inhibitors. The presence of PgP, BCRP, MRP-1 has been confirmed in the BeWo b30 cells (Atkinson et al., 2003; Ceckova et al., 2006; Evseenko et al., 2006; Milane et al., 2009; Mitra and Audus, 2010; Wick et al., 2010) but inhibitors of PgP and BCRP at a concentration of 50 and 2.5 μ M, respectively, showed no effect on translocation of PS-NPs across the BeWo b30 cell layers. MK571 (24 μ M), an inhibitor of MRP-1, significantly increased the basolateral translocation of positively charged PS-NP by 1.5 fold but did not influence the translocation of the negatively charged PS-NPs so in general the translocation of the PS-NPs tested appeared to occur preferentially by passive diffusion.

In vitro models are attractive for high throughput testing of various NPs. However, it should be kept in mind that in vitro models like the BeWo b30 transwell model applied in the current study have their limitations (Nikitina et al., 2013). For example, given that the physiology of the placental barrier in vivo varies in time,

it is difficult to classify the BeWo cell layer in a representing specific stage of pregnancy. Furthermore, the BeWo transwell model is a simplified placental barrier compared to the complex in vivo placental barrier since it lacks the multiple layers of different cell types (cytotrophoblasts and syncytiotrophoblasts) and extracellular matrix including collagen, known to constitute the in vivo placental barrier. This implies that extrapolation of in vitro results to the in vivo situation should acknowledge uncertainties in the predictions made (Mathiesen et al., 2014). To this end we have included the model compounds amoxicillin and antipyrine, known to be translocated across the placental barrier to respectively only a limited or large extent (Akbaraly et al., 1985; Li et al., 2013) to enable qualitative interpretation of the results. This comparison revealed that for positively charged PS-NPs translocation was 17 fold lower and for negatively charged PS-NPs from Polysciences 2.5 fold higher than that of amoxicillin, while for the negatively charged PS-NPs from Magsphere no translocation was found under the same test conditions.

In conclusion, the translocation studies of PS-NPs in the present study and the comparison of the data with translocation data of model compounds, for which the model has been validated with an ex vivo placental model, reveal that the in vitro BeWo b30 model can be used as a fast method to get an initial qualitative impression about the capacity of NPs to translocate across the placental barrier and set priorities for further in vivo studies on translocation of NPs to the fetus.

Conflict of Interest

The authors report no conflict of interest.

Transparency Document

The Transparency document associated with this article can be found in the online version.

Acknowledgements

This work is supported by NanoNextNL, a micro and nanotechnology consortium of the Government of The Netherlands and 130 partners.

Appendix A. Supplementary material

Supplementary data associated with this article can be found, in the online version, at <http://dx.doi.org/10.1016/j.tiv.2015.07.003>.

References

- Akbaraly, J.P., Guibert, S., Leng, J.J., Auzerie, J., 1985. Transplacental transfer of 5 antibiotics by in vitro human placental perfusion. *Pathol. Biol. (Paris)* 33, 368–372.
- Ali, H., Kalashnikova, I., White, M.A., Sherman, M., Rytting, E., 2013. Preparation, characterization, and transport of dexamethasone-loaded polymeric nanoparticles across a human placental in vitro model. *Int. J. Pharm.* 454, 149–157.
- Arora, A., Padua, G.W., 2010. Review: nanocomposites in food packaging. *J. Food Sci.* 75, R43–R49.
- Artursson, P., Karlsson, J., 1991. Correlation between oral drug absorption in humans and apparent drug permeability coefficients in human intestinal epithelial (Caco-2) cells. *Biochem. Biophys. Res. Commun.* 175, 880–885.
- Atkinson, D.E., Greenwood, S.L., Sibley, C.P., Glazier, J.D., Fairbairn, L.J., 2003. Role of MDR1 and MRP1 in trophoblast cells, elucidated using retroviral gene transfer. *Am. J. Physiol. Cell Physiol.* 285, C584–C591.
- Auffan, M., Rose, J., Bottero, J.Y., Lowry, G.V., Jolivet, J.P., Wiesner, M.R., 2009. Towards a definition of inorganic nanoparticles from an environmental, health and safety perspective. *Nat. Nanotechnol.* 4, 634–641.

- Avery, M.L., Meek, C.E., Audus, K.L., 2003. The presence of inducible cytochrome P450 types 1A1 and 1A2 in the BeWo cell line. *Placenta* 24, 45–52.
- Bhattacharjee, S., Ershov, D., Gucht, J.V., Alink, G.M., Rietjens, I.M., Zuilhof, H., Marcelis, A.T., 2011. Surface charge-specific cytotoxicity and cellular uptake of tri-block copolymer nanoparticles. *Nanotoxicology*.
- Bhattacharjee, S., Ershov, D., Fytianos, K., Gucht, J., Alink, G., Rietjens, I., Marcelis, A., Zuilhof, H., 2012. Cytotoxicity and cellular uptake of tri-block copolymer nanoparticles with different size and surface characteristics. Part. Fibre Toxicol. 9, 11.
- Bhattacharjee, S., Rietjens, I.M., Singh, M.P., Atkins, T.M., Purkait, T.K., Xu, Z., Regli, S., Shukaliak, A., Clark, R.J., Mitchell, B.S., Alink, G.M., Marcelis, A.T., Fink, M.J., Veinot, J.G., Kauzlarich, S.M., Zuilhof, H., 2013a. Cytotoxicity of surface-functionalized silicon and germanium nanoparticles: the dominant role of surface charges. *Nanoscale* 5, 4870–4883.
- Bhattacharjee, S., van Opstal, E.J., Alink, G.M., Marcelis, A.T.M., Zuilhof, H., Rietjens, I.M.C.M., 2013b. Surface charge-specific interactions between polymer nanoparticles and ABC transporters in Caco-2 cells. *J. Nanopart. Res.* 15.
- Bode, C.J., Jin, H., Ryttig, E., Silverstein, P.S., Young, A.M., Audus, K.L., 2006. In vitro models for studying trophoblast transcellular transport. *Methods Mol. Med.* 122, 225–239.
- Brand, W., van der Wel, P.A., Rein, M.J., Barron, D., Williamson, G., van Bladeren, P.J., Rietjens, I.M., 2008. Metabolism and transport of the citrus flavonoid hesperetin in Caco-2 cell monolayers. *Drug Metab. Dispos.* 36, 1794–1802.
- Buerki-Thurnher, T., von, M., Wick, P., 2012. Knocking at the door of the unborn child: engineered nanoparticles at the human placental barrier. *Swiss Med Wkly* 142.
- Cartwright, L., Poulsen, M.S., Nielsen, H.M., Pojana, G., Knudsen, L.E., Saunders, M., Ryttig, E., 2012. In vitro placental model optimization for nanoparticle transport studies. *Int. J. Nanomed.* 7, 497–510.
- Ceckova, M., Libra, A., Pavek, P., Nachtigal, P., Brabec, M., Fuchs, R., Staud, F., 2006. Expression and functional activity of breast cancer resistance protein (bcrp, abcg2) transporter in the human choriocarcinoma cell line BeWo. *Clin. Exp. Pharmacol. Physiol.* 33, 58–65.
- Chiu, H.W., Xia, T., Lee, Y.H., Chen, C.W., Tsai, J.C., Wang, Y.J., 2015. Cationic polystyrene nanospheres induce autophagic cell death through the induction of endoplasmic reticulum stress. *Nanoscale* 7, 736–746.
- Correia Carreira, S., Walker, L., Paul, K., Saunders, M., 2013. The toxicity, transport and uptake of nanoparticles in the in vitro BeWo b30 placental cell barrier model used within NanoTEST. *Nanotoxicology*.
- dos Santos, T., Varela, J., Lynch, I., Salvati, A., Dawson, K.A., 2011. Effects of transport inhibitors on the cellular uptake of carboxylated polystyrene nanoparticles in different cell lines. *PLoS One* 6, e24438.
- Evesenko, D.A., Paxton, J.W., Keelan, J.A., 2006. ABC drug transporter expression and functional activity in trophoblast-like cell lines and differentiating primary trophoblast. *Am. J. Physiol. – Regul. Integr. Comp. Physiol.* 290, R1357–R1365.
- Grafmuller, S., Manser, P., Krug, H.F., Wick, P., von Mandach, U., 2013. Determination of the transport rate of xenobiotics and nanomaterials across the placenta using the ex vivo human placental perfusion model. *J. Vis. Exp.*
- Juch, H., Nikitina, L., Debbage, P., Dohr, G., Gauster, M., 2013. Nanomaterial interference with early human placenta: sophisticated matter meets sophisticated tissues. *Reprod. Toxicol.* 41, 73–79.
- Kim, W.J., Bonoiu, A.C., Hayakawa, T., Xia, C., Kakimoto, M.A., Pudavar, H.E., Lee, K.S., Prasad, P.N., 2009. Hyperbranched polysiloxane nanoparticles: surface charge control of nonviral gene delivery vectors and nanoprobe. *Int. J. Pharm.* 376, 141–152.
- Lee, J.Y., Kim, J.S., Cho, H.J., Kim, D.D., 2014. Poly(styrene)-b-poly(DL-lactide) copolymer-based nanoparticles for anticancer drug delivery. *Int. J. Nanomed.* 9, 2803–2813.
- Lesniak, A., Campbell, A., Monopoli, M.P., Lynch, I., Salvati, A., Dawson, K.A., 2010. Serum heat inactivation affects protein corona composition and nanoparticle uptake. *Biomaterials* 31, 9511–9518.
- Li, H., van Ravenzwaay, B., Rietjens, I.M., Louisse, J., 2013. Assessment of an in vitro transport model using BeWo b30 cells to predict placental transfer of compounds. *Arch. Toxicol.* 87, 1661–1669.
- Liu, F., Soares, M.J., Audus, K.L., 1997. Permeability properties of monolayers of the human trophoblast cell line BeWo. *Am. J. Physiol. – Cell Physiol.* 273, C1596–C1604.
- Liu, W., Rose, J., Plantevin, S., Auffan, M., Bottero, J.Y., Vidaud, C., 2013a. Protein corona formation for nanomaterials and proteins of a similar size: hard or soft corona? *Nanoscale* 5, 1658–1668.
- Liu, X., Huang, N., Li, H., Jin, Q., Ji, J., 2013b. Surface and size effects on cell interaction of gold nanoparticles with both phagocytic and nonphagocytic cells. *Langmuir* 29, 9138–9148.
- Lundqvist, M., Stigler, J., Elia, G., Lynch, I., Cedervall, T., Dawson, K.A., 2008. Nanoparticle size and surface properties determine the protein corona with possible implications for biological impacts. *Proc. Natl. Acad. Sci.* 105, 14265–14270.
- Mathiesen, L., Morck, T.A., Zuri, G., Andersen, M.H., Pehrson, C., Frederiksen, M., Mose, T., Ryttig, E., Poulsen, M.S., Nielsen, J.K., Knudsen, L.E., 2014. Modelling of human transplacental transport as performed in Copenhagen, Denmark. *Basic Clin. Pharmacol. Toxicol.*
- Menjoge, A.R., Rinderknecht, A.L., Navath, R.S., Faridnia, M., Kim, C.J., Romero, R., Miller, R.K., Kannan, R.M., 2011. Transfer of PAMAM dendrimers across human placenta: prospects of its use as drug carrier during pregnancy. *J. Control. Release* 150, 326–338.
- Milane, A., Vautier, S., Chacun, H., Meininger, V., Bensimon, G., Farinotti, R., Fernandez, C., 2009. Interactions between riluzole and ABCG2/BCRP transporter. *Neurosci. Lett.* 452, 12–16.
- Mitra, P., Audus, K.L., 2010. MRP isoforms and BCRP mediate sulfate conjugate efflux out of BeWo cells. *Int. J. Pharm.* 384, 15–23.
- Myllynen, P.K., Loughran, M.J., Howard, C.V., Sormunen, R., Walsh, A.A., Vahakangas, K.H., 2008. Kinetics of gold nanoparticles in the human placenta. *Reprod. Toxicol.* 26, 130–137.
- Nikitina, L., Dohr, G., Juch, H., 2013. Studying nanoparticle interaction with human placenta: Festina lente! *Nanotoxicology*.
- Oberdorster, E., 2004. Manufactured nanomaterials (fullerenes, C60) induce oxidative stress in the brain of juvenile largemouth bass. *Environ. Health Perspect.* 112, 1058–1062.
- Oberdorster, G., Oberdorster, E., Oberdorster, J., 2005. Nanotoxicology: an emerging discipline evolving from studies of ultrafine particles. *Environ. Health Perspect.* 113, 823–839.
- Park, M.V., Neigh, A.M., Vermeulen, J.P., de la Fonteyne, L.J., Verharen, H.W., Briede, J.J., van Loveren, H., de Jong, W.H., 2011. The effect of particle size on the cytotoxicity, inflammation, developmental toxicity and genotoxicity of silver nanoparticles. *Biomaterials* 32, 9810–9817.
- Phosphorex, Commercial Applications Use Polystyrene Nanoparticles, 2013. <<http://www.phosphorex.com/1/post/2013/07/commercial-applications-use-polystyrene-nanoparticles.html>>.
- Poulsen, M.S., Ryttig, E., Mose, T., Knudsen, L.E., 2009. Modeling placental transport: correlation of in vitro BeWo cell permeability and ex vivo human placental perfusion. *Toxicol. In Vitro: Int. J. Published Assoc. BIBRA* 23, 1380–1386.
- Sager, T.M., Castranova, V., 2009. Surface area of particle administered versus mass in determining the pulmonary toxicity of ultrafine and fine carbon black: comparison to ultrafine titanium dioxide. Part Fibre Toxicol. 6, 15.
- Saunders, M., 2009. Transplacental transport of nanomaterials. *Wiley Interdiscip. Rev. Nanomed. Nanobiotechnol.* 1, 671–684.
- Simon, P., Chaudhry, Q., Bakos, D., 2008. Migration of engineered nanoparticles from polymer packaging to food – a physicochemical view. *J. Food Nutr. Res.* 47, 105–113.
- Sonnegaard Poulsen, M., Mose, T., Leth Maroun, L., Mathiesen, L., Ehlert Knudsen, L., Ryttig, E., 2013. Kinetics of silica nanoparticles in the human placenta. *Nanotoxicology*.
- Stampfli, A., Maier, M., Radykewicz, R., Reitmeir, P., Göttlicher, M., Niessner, R., 2011. Langendorff heart: a model system to study cardiovascular effects of engineered nanoparticles. *ACS Nano* 5, 5345–5353.
- Takeuchi, Y., Sakakibara, R., Ishiguro, M., 1990. Synthesis and secretion of human chorionic gonadotropin and its subunits in choriocarcinoma cells: a comparative study with normal placental cells. *Mol. Cell. Endocrinol.* 69, 145–156.
- Ushigome, F., Takanaga, H., Matsuo, H., Yanai, S., Tsukimori, K., Nakano, H., Uchiumi, T., Nakamura, T., Kuwano, M., Ohtani, H., Sawada, Y., 2000. Human placental transport of vinblastine, vincristine, digoxin and progesterone: contribution of P-glycoprotein. *Eur. J. Pharmacol.* 408, 1–10.
- Utoguchi, N., Chandorkar, G.A., Avery, M., Audus, K.L., 2000. Functional expression of P-glycoprotein in primary cultures of human cytotrophoblasts and BeWo cells. *Reprod. Toxicol.* 14, 217–224.
- Walczak, A.P., Kramer, E., Hendriksen, P.J., Tromp, P., Helsper, J.P., van der Zande, M., Rietjens, I.M., Bouwmeester, H., 2014. Translocation of differently sized and charged polystyrene nanoparticles in *in vitro* intestinal cell models of increasing complexity. *Nanotoxicology*, 1–9.
- Wick, P., Malek, A., Manser, P., Meili, D., Maeder-Althaus, X., Diener, L., Diener, P.A., Zisch, A., Krug, H.F., von Mandach, U., 2010. Barrier capacity of human placenta for nanosized materials. *Environ. Health Perspect.* 118, 432–436.